

OPEN ACCESS

Self-heating forecasting for thick laminate specimens in fatigue

To cite this article: F Lahuerta *et al* 2014 *J. Phys.: Conf. Ser.* **555** 012062

View the [article online](#) for updates and enhancements.

You may also like

- [A novel meshfree method for three-dimensional natural frequency analysis of thick laminated conical, cylindrical shells and annular plates](#)
Songhun Kwak, Kwanghun Kim, Kwangil An et al.
- [Effects of shape and direction of osteocyte lacunae on stress distribution of osteon](#)
Yuxi Liu, Gongxing Yan, Song Chen et al.
- [Manufacturing curing cycles influence on local fracture toughness properties at micro and macro scale](#)
F Lahuerta and S Raijmaekers



ECS
The
Electrochemical
Society
Advancing solid state &
electrochemical science & technology

DISCOVER
how sustainability
intersects with
electrochemistry & solid
state science research

Self-heating forecasting for thick laminate specimens in fatigue

F. Lahuerta, T. Westphal, R.P.L. Nijssen

Knowledge Centre WMC, 1770 AA Wieringerwerf The Netherlands

E-mail: f.lahuerta@wmc.eu | t.westphal@wmc.eu | r.p.l.nijssen@wmc.eu

Abstract. Thick laminate sections can be found from the tip to the root in most common wind turbine blade designs. Obtaining accurate and reliable design data for thick laminates is subject of investigations, which include experiments on thick laminate coupons. Due to the poor thermal conductivity properties of composites and the material self-heating that occurs during the fatigue loading, high temperature gradients may appear through the laminate thickness. In the case of thick laminates in high load regimes, the core temperature might influence the mechanical properties, leading to premature failures. In the present work a method to forecast the self-heating of thick laminates in fatigue loading is presented. The mechanical loading is related with the laminate self-heating, via the cyclic strain energy and the energy loss ratio. Based on this internal volumetric heat load a thermal model is built and solved to obtain the temperature distribution in the transient state. Based on experimental measurements of the energy loss factor for 10mm thick coupons, the method is described and the resulting predictions are compared with experimental surface temperature measurements on 10 and 30mm UD thick laminate specimens.

1. Introduction

To date, wind turbine blade designs are based on static and fatigue tests on 1-5mm thick coupons, safety factors established by the certification entities, root joint tests and full scale blade tests. Very limited work on the differences between thin and thick laminates in fatigue or static tests [1-4].

Literature reports different factors related to the scaling effects between thin and thick coupons. Examples of these effects are size and scaling factors [5,6], residual stresses [7] due to the manufacturing process and test effects or edge factors [3,4]. Stammes theorises [2] that the temperature build-up that appears in thick laminates fatigue tests might lead to premature failures due to the high temperatures.

The aim of this work is to describe a method to forecast the temperature rise in thick laminate coupons during fatigue loading, in order to take this factor into account and optimise thick laminate test design.

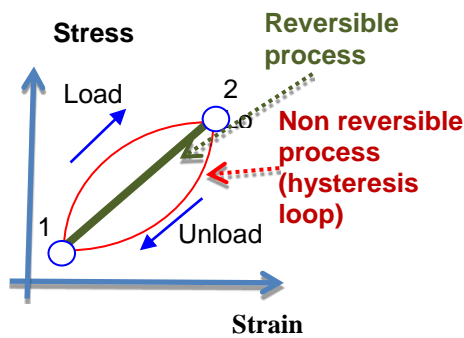
It has been reported that in composite materials a percentage of the mechanical loading and unloading strain energy density is transformed into heat due to non-reversible processes [8,9]. Part of the mechanical loading energy per cycle is not returned mechanically, but is transformed into heat, also called intrinsic dissipation [10-12]. The non-reversible processes that occur during the cyclic loading are related with different processes such as viscoelasticity, matrix plastic deformation, crack onset and propagation, internal friction or fibre breakage. These processes are the cause of a progressive change of the state or structure of the material (effective stress and strain) and therefore a change in the internal energy that a given volume of material has. The energy release leads to the



“endogenous heating” or “self-generated heating” of the material, which is the cause of the temperature rise in fatigue. Since the cyclic mechanical loading and the internal volumetric heat can be correlated via the damping ratio or loss factor [13,14], the determination of the thermal loads allows to solve the transient thermal problem and the temperature distribution.

1.1. Analytical problem

In figure 1, potential stress-strain during cyclic loading are shown. Taking into account that during each loading cycle a hysteresis loop is developed due to non-reversible processes, the strain energy introduced between point 1 and 2 and the energy strain return between 2 and 1 are not equal. Thus, there is a loss of mechanical energy in the process that can be defined by equation (1). The energy loss during the cycle ΔW_{loss} is related with the cyclic elastic energy according to the loss factor. Some authors have related the loss factor or damping capacity in composites with the amplitude decay in vibration tests at the natural frequency [15–17]. However, the loss factor or damping factor is formally defined as the ratio of energy loss and elastic strain energy (2) [8,13]. This can be related to the mechanical energy that the real system consumes in addition to what the linear elastic model predicts.



$$\Delta W_{loss} = W_{1-2}^{load-nonrev} - W_{1-2}^{unload-nonrev} \quad (1)$$

$$\phi = \frac{\Delta W_{loss}}{W_{1-2}^{load-rev}} \quad (2)$$

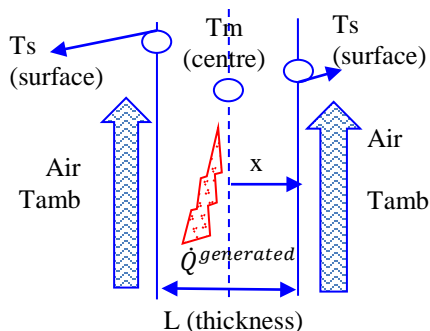
$$\Delta W_{loss} = Q_{1-2-1}^{generated} + E_{1-2-1}^{surface} \approx Q_{1-2-1}^{generated} \quad (3)$$

$$\dot{Q}^{generated} = f \cdot \phi \cdot W_{1-2}^{load-rev} \quad (4)$$

Where ΔW_{loss} is the cyclic loss energy and $W_{1-2}^{load-nonrev}$ and W_{1-2}^{unload} unload energy strain

Figure 1. Diagram between reversible and non-reversible processes (hysteresis cycle)

The mechanical energy loss is transformed into internal heat $Q_{1-2-1}^{generated}$ and new surface energy $E_{1-2-1}^{surface}$, however the new surface energy term can be assumed as very small [18,19]. Thus, the hysteresis energy loss ΔW_{loss} can be assumed equal to the internal heat generated per cycle $\dot{Q}^{generated}$ (3). In this way it is possible to link the mechanical model with the thermal model during the cyclic loading. Therefore, the volumetric internal heat flow that appears during the cyclic loading can be expressed as equation (4), as function of the elastic strain energy density $W_{1-2}^{load-rev}$.



$$T_m = f \cdot \phi \cdot \frac{\sigma_2^2 - \sigma_1^2}{E_{12}} \cdot \left(\frac{L^2}{4 \cdot k} + \frac{L}{2 \cdot h} \right) + T_\infty \quad (5)$$

Where, σ_2, σ_1 : max and min tension, E_{12} elastic modulus, ϕ loss factor, f frequency, T_∞ ambient temperature, L thickness, k conductivity, h convection coefficient

Figure 2. 1D thermal model diagram for a coupon in dynamic loading

The problem of a coupon tested in fatigue can be studied analytically according to the one-dimensional heat transfer theory [20], based on a 1D plane wall with an internal uniform volumetric heat generation (see figure 2), where the temperature distribution through the thickness in the coupon is defined by equation (5). The following assumptions are considered in the 1D solution: the width and the length are considered infinite, the loss factor stays constant in time and space, the strain energy

stays constant in time and space, isotropic and uniform conductivity properties, symmetric boundary conditions, and only the strain energy in the main loading direction is considered.

2. FEM methodology

Although the 1D analytical solution offers a coarse approach to describe the laminate’s self-heating, it gives an intuitive understanding of the problem. In most cases 1D assumptions are not valid and the use of FEM is required. For those cases a FEM methodology to evaluate the self-heating of thick laminates is proposed.

Initially the problem to solve is a mechanical problem coupled with a thermal problem, in which an internal volumetric heat at each element depends linearly on the strain energy density scalar field via the loss factor (4). In addition, the loss factor might vary per element due to ply orientation and damage evolution [21], hence for each element, a different loss factor might be used based on its material or ply orientation. The simultaneous solution of the thermal and mechanical problem presents two problems:

First, the time scale between the mechanical and the thermal problem is of a different order. While the mechanical problem’s main frequency might vary between 0.5 to 2Hz, the thermal stability is achieved after 10 minutes to 2 hours, therefore the time steps differ by an order of two.

The second problem is that the FEM solver does not allow to impose an internal heat flow dependent on the strain energy generated in each time step.

To circumvent these problems, the mechanical and thermal problem can be solved separately (uncoupled). In this way, the steps to solve the problem can be presented as (see figure 3):

- Solve the mechanical problem for one loading cycle as a quasi-static simulation with a representative time step of the mechanical frequency.
- Extract the strain energy scalar field
- Integrate the strain energy for a half cycle (elastic strain energy) and each element of the mesh, for all the tensor components.

$$W_{1-2}^{load-rev}(x, y, z) = \int_1^2 \sigma(x, y, z) \cdot d\varepsilon, \forall x, y, z$$

- Multiply by the loss factor to obtain the internal heat generation.

$$\dot{Q}^{generated}(x, y, z) = f \cdot \phi(x, y, z) \cdot W_{1-2}^{load-rev}(x, y, z)$$

- Build the thermal problem with the same mesh.
- Import the internal heat generation as a volumetric internal heat load at each different mesh element of the thermal problem.
- Solve the thermal problem with a representative time step of the temperature evolution

This methodology is based on the following assumptions: the loss factor stays constant during most of the test, the changes in the strain energy scalar field are small with respect to the cyclic loading time and the free surface energy generation is not taken into consideration. In addition, detailed considerations of the variation of the loss factor due to ply orientation might be considered according to the methodology, however in coupon testing ply orientation is mainly uniform unless in the tab region close to the steel grips.

Based on Infra-red (IR) camera observations, minor local temperature increase was observed in the crack tip regions for the coupons in the case that a crack between the test specimen and the tab

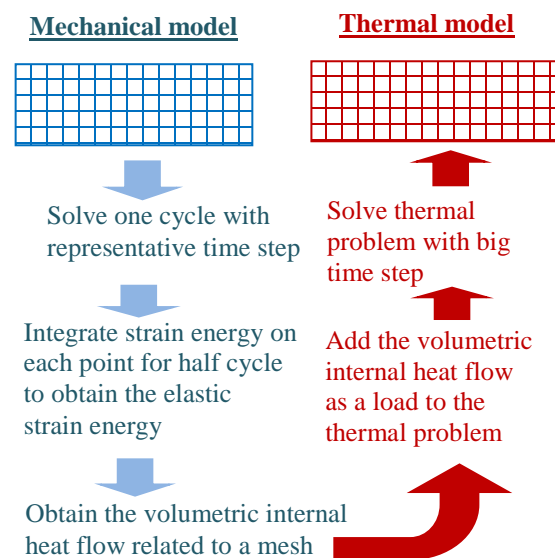


Figure 3. Temperature self-heating FEM forecast methodology flow task diagram

appears. However due to its proximity to the steel grips and its local nature in comparison with the full volume of the specimen, this effect was not considered in the FEM simulations.

3. Materials and methods

Different fatigue test coupons are used in order to validate the methodology. Three different fatigue test configurations (see figure 4) are studied recording the temperature rise during the test and applying the FEM methodology described above.

- The Optimat [2] S07 UD tension coupons, 30mm thick;
- The S77 transverse direction compression coupons, 30mm thick;
- The S20 UD end loading compression coupons, 10mm thick.

The hysteresis loss factor was measured during the tests based on the hysteresis areas. The hysteresis loss factors were used subsequently as the loss factor for the FEM models. Along the tests, small changes of the hysteresis loss factors were observed shortly before failure of the specimens.

3.1. S07 UD tension coupon

The epoxy glass fiber UD coupon GEV314_S0700_0003 is tested at $R=0.1$ for 196 MPa during the Optimat project [2]. The evolution of the temperature was measured with thermocouples in the tab position and between the tabs. Initially, the test frequency was set-up at 0.3 Hz, but after an initial temperature rise of 15°C at 5000 cycles it was decreased to 0.2 Hz. The ambient temperature was 20°C.

The mechanical FE model is performed on one eighth of the geometry, in such way that a symmetry plane condition in the transversal centre plane, the centre thickness plane and the longitudinal centre plane is imposed with restricted displacements at each plane in the normal direction of the planes. In order to simulate the loading cycle at the holes (in the tab region of the S07 specimens) in a simple way, the global loading is distributed over the four holes (assuming same distribution coefficients), and a bearing load is imposed based on a cosine-shaped pressure distribution. Additionally, the pressure load distribution is multiplied by a time-dependent sinusoidal function with a frequency of 0.3Hz. The material properties are representative for a mainly UD orthotropic glass fiber epoxy composite, the modulus in the main direction is assumed to be 31.5 GPa [2]. The mesh is based on 86,900 tetrahedron elements.

The stress and strain fields obtained from the mechanical FE model are processed with a Python code in order to calculate the strain energy density for the whole cycle. A loss factor of 0.04 is assumed for this purpose, according to the S20 geometry tests.

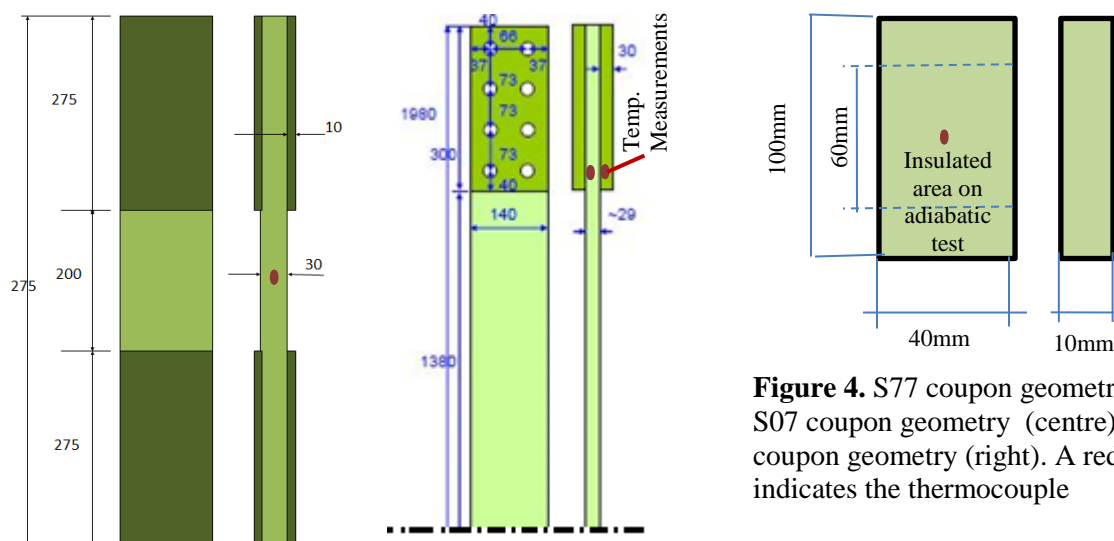


Figure 4. S77 coupon geometry (left). S07 coupon geometry (centre). S20 coupon geometry (right). A red dot indicates the thermocouple

The thermal FE model is based on the same geometry and mesh as the mechanical FE model. The material definition is an isotropic material with a conductivity of $0.512 \text{ W/m}^\circ\text{C}$ and a specific heat of $1044 \text{ J/kg}^\circ\text{C}$. The conductivity and specific heat are calculated according to a rule of mixtures-based approach proposed by Cugnet [22]. An initial uniform solid and air temperature of 20°C is considered, and a convection boundary condition for all the (non-symmetry plane) surfaces is imposed. As the convection coefficient is not a well-characterised value, a sensitivity analysis for different convection coefficient values between 10 to $20 \text{ W/m}^2^\circ\text{C}$ is carried out.

3.2. S77 transverse direction compression coupon

The epoxy glass fiber 30mm thick transverse direction coupons S77900-4 and S77900-9 are tested in compression-compression fatigue, at $R=10$ and 105MPa maximum compressive stress, with a frequency of 0.25Hz and 0.5Hz , respectively (see figure 5). In both cases the surface temperature is monitored with the IR camera, showing a stable surface temperature of 33°C and $42\text{-}45^\circ\text{C}$, respectively, during most of the test. Also the temperature is measured with a thermocouple on one side of the coupon.

The hysteresis loss factor is measured during the test. In all cases the loss factor shows a constant behaviour during most of the coupon life. To obtain a single value for use in the numerical calculation, The average loss factor for first/middle 60% of fatigue life is extracted from the measurements, also avoiding the exponential rise that occurs at the end of the coupon life (in the last degradation phase).

The coupon geometry is simplified for the mechanical FE model in the same way as the S07 geometry, three symmetry planes with the displacement constraints. The shear loading carried out by the grips is translated to an equivalent shear load in the gripping surface. The material properties are those of the S07 configuration, rotated 90 degrees with a transverse modulus of 13.5 GPa (value measured). The mesh is based on 8710 solid Marc Hex8 elements.

The stress and strain fields obtained from the mechanical FE model are processed with a Python code in order to calculate the strain energy loss for the whole cycle. An average loss factor of 0.06 is taken from four coupons (see table 3).

The thermal model is based on the same conductivity, specific heat, and solid and air temperature that the S07 configuration used. The boundary conditions for the thermal model are:

- A convection boundary condition in all the surfaces with no symmetry planes or gripping surface. A sensitivity analysis for different convection coefficient values is carried out between 5 to $15 \text{ W/m}^2^\circ\text{C}$;
- A contact resistance condition with a solid at 20°C is imposed on the gripping area. The contact resistance condition is considered of $2 \cdot 10^4 \text{ m}^2^\circ\text{C/W}$ [23]. A sensitivity analysis for this value is carried out, showing differences in the temperature results not higher than 2 degrees for a contact resistance four orders different;
- A volumetric internal heat based on the mechanical model calculations.

3.3. S20 UD compression coupon

Twenty S20 end loading compression coupons 10mm thick are tested in $R=10$ fatigue for different loads at 1.5Hz (see figure 5). Half of the coupons are tested in normal conditions and half of the



Figure 5. Top: S77 test configuration and failure mode. Bottom: S20 test configuration

coupons with the surface covered by insulation material. Hysteresis loss factor measurements are carried out during the test and the surface area temperature is recorded via thermocouples.

The higher load coupon TO04S20 in insulated conditions is tested at 285MPa max compression showing a surface temperature between 32-35°C. A FE model for this coupon geometry is built in the same way as explained for the S07 and S77 geometries, with a resistance contact boundary condition in the non-insulated area. The insulated material conductivity is 0.023 W/m°C [24] and the convection coefficient is assumed as 15 W/m²°C.

4. Results and discussion

The temperature evolution for the thick laminates fatigue tests is compared with the thermal models based on the self-heating FEM forecast methodology described in the present work. In the following section the experimental and model results are compared and discussed.

4.1. S20 UD compression coupon

The model temperatures of the S20 coupon at the surface are around 35-40°C and around 40-45°C in the core. Taking into account that coupon TO04S20 is tested at higher loads, the model predicts that no temperatures above the operational range of the material occur during the S20 coupon fatigue tests, whether insulated or non-insulated. This agrees with the fatigue life experimental data, which do not show important differences between the insulated and non-insulated coupons (see figure 6). However higher increments might lead into changes of the mechanical properties [25].

4.2. S07 UD tension coupon results

In table 1 the experimental and model temperatures are shown in the steady state for three different convection coefficients. As the thermocouple measurements are taken on the coupons' side faces in the gripping area, the model temperatures in the external gripping area surface are compared with them. The best match of the experimental temperatures in the steady state and for the transient state arrival time is with a convection coefficient of 15 W/m°C. Additionally, table 1 also shows that there is a strong non-conservative difference between the 1D model temperatures and the FEM temperatures, probably because of the strong assumptions associated with the 1D model.

The experimental time to arrive to the steady state measured in the grip area, agrees with the steady state time of the model for the same location, which is around 5000 cycles. In figure 7 the temperature gradients are shown at 5000 cycles near the steady state. It is interesting

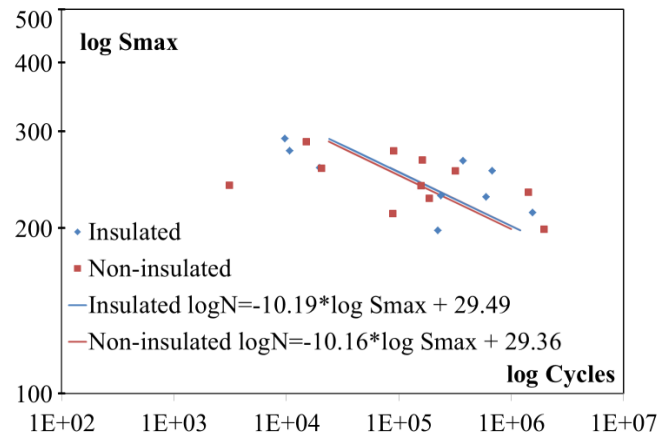


Figure 6. S-N curve S20 tests

Table 1. FEM and experimental reference temp. in the steady state for S07 configuration

Conv. Factor (W/m°C)	T Btw. Tabs (°C)	T in tab (°C)	T centre (°C)	T centre 1D theory (°C)	T (°C) Exp. (2 sensor signal)
10	37	33	71	33	30-35
15	32	30	57	29	
20	27	24	50	27	

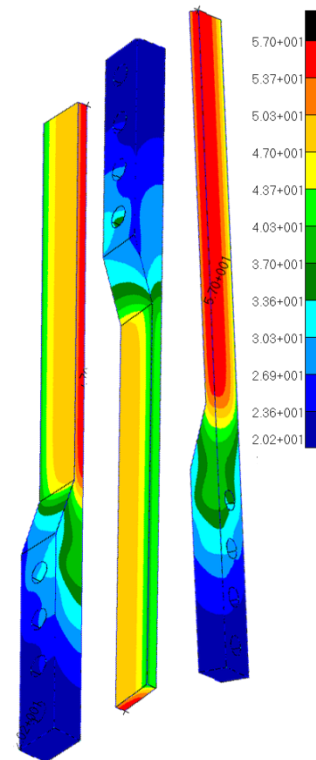


Figure 7. Temperature field in the steady state (convection factor 15 W/m°C, Units: °C, at 5000 cycles, 0.3 Hz, three different solid views).

to see how the temperature field corresponds with the tension field. Taking into account the wide range of convection coefficients chosen (between 10-20 W/m²C) it can be said that the core temperature can be safely estimated between 50 to 70°C. The frequency during the test was reduced to 0.2Hz to prevent excessive self-heating during the test [2].

Table 2. FEM and experimental reference temperatures in the steady state for S77900-4 and S77900-9 coupons

Freq. (Hz)	Conv. Factor (W/m ² C)	T side (°C)	T surface (°C)	T centre (°C)	1D T centre theory (°C)	T (°C) Experimental
0.25	5	37	41	43	33	33-36 (IR)
	10	28	31	33	27	
	15	25	27	30	25	
0.5	5	55	61	66	46	45-47 (IR)
	10	36	42	47	34	
	15	30	35	38	30	

Table 3. 30 mm thick compression coupons data, R=10 test at 0.25Hz and 0.5Hz

Coupon ID S77900	Freq. (Hz)	Max stress (MPa)	Cycles	Loss factor	T avg IR camera (°C)	T max Surface Thermo couple (°C)
6	0.25	115.5	63,927	-	-	26
3	0.25	109.5	153,922	0.0591	-	25
4 ^a	0.25	105.0	404,891	0.0601	33-36	27
1	0.50	115.5	6,300	-	55-60	40
2	0.50	109.5	18,809	0.0641	46-50	35
9	0.50	105.0	22,014	0.0638	45-47	30

^a Run-out

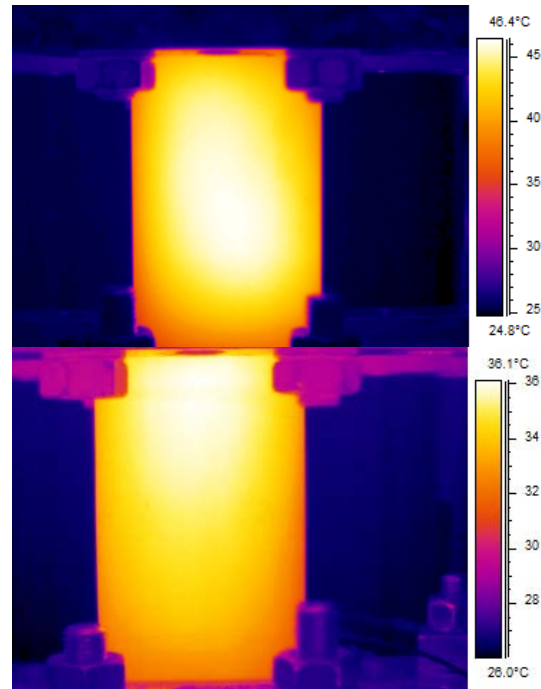


Figure 8. Top: IR thermal image of S779-9 at half of the fatigue life (R=10, 105 MPa, 0.5Hz). Bottom: IR thermal image of S779-4 at half of the fatigue life (R=10, 105 MPa, 0.25Hz)

4.3. S77 transverse direction compression coupon results

In table 2 the S77900-4 (0.25 Hz) and the S77900-9 (0.5Hz) steady state thermal model temperatures are shown for convection coefficients between 5-15 W/m²C, and the experimental surface IR temperature measurement (see figure 8). The best match of the experimental temperatures in the steady state is for a convection coefficient of 10 W/m²C. While the S77 coupon is tested without air cooling units, the S07 is tested with cooling units; hence the difference between the convection coefficients. Additionally, table 2 shows that also in this case there is a strong non-conservative difference with the 1D model temperatures.

For the convection coefficient range taken into consideration (5-15 W/m²C), the model shows temperature ranges in the core between 47 to 66°C for the 0.5Hz coupon and between 33 to 43°C for the 0.25 Hz coupon. The implications of temperature rise are shown in table 3, where it can be seen that the fatigue life obtained at 0.25Hz exceeds the 0.5Hz fatigue life by one order of magnitude. In addition, the thermocouples installed on one side (see table 3) yield temperatures that are in the order of the ones in the model, but do not give an accurate idea of the temperatures inside the coupon due to the scale of the coupon and the broad temperature distribution that can be registered.

5. Conclusions

A finite element methodology to forecast the temperature distribution in the thick laminates fatigue test is described in the present work, linking the hysteresis loss factor and the strain energy density

with the internal volumetric heat. The methodology is validated against experimental data of different coupon configurations and fatigue tests. In addition, evidence of premature failures in thick laminates fatigue tests due to excessive temperature in the laminate core are reported. The result of this study facilitates thick laminates fatigue test design.

References

- [1] Wingerde A van, Stammes E, Nijssen R P L and Westphal T 2006 *2500 kN test set-up for thick laminates WP10 Optimat blades. Report OB_TG4_R015* (Knowledge centre WMC, Wiringerwerf NL)
- [2] Stammes E, Nijssen R P L and Westphal T 2010 *Effect of laminate thickness tests on thick laminates. Report WMC-2009-38* (Wiringerwerf NL)
- [3] E.T. Camponeschi 1989 *Compression Testing of Thick-Section Composite Materials DTRC-SME-8* (David Taylor Research Centre, Maryland USA)
- [4] Hsiao H M, Daniel I M and Wooh S C 1995 A New Compression Test Method for Thick Composites *J. Compos. Mater.* **29** 1789–806
- [5] Sutherland L S, Sheno R A and Lewis S M 1999 Size and scale effects in composites: I. Literature review *Compos. Sci. Technol.* **59** 209–20
- [6] Sutherland L S, Sheno R A and Lewis S M 1999 Size and scale effects in composites: II. Unidirectional laminates *Compos. Sci. Technol.* **59** 221–33
- [7] Withers P J and Bhadeshia H K D H 2001 Residual stress Part 1 – Measurement techniques *Mater. Sci. Technol.* **17** 355–65
- [8] Ratner S B and Korobov V I 1966 Self-heating of plastics during cyclic deformation *Polym. Mech.* **1** 63–8
- [9] Reifsnider K L and Williams R S 1974 Determination of fatigue-related heat emission in composite materials during fatigue loading *Exp. Mech.* **14** 479–85
- [10] Redon O 2000 *Fatigue damage development and failure in unidirectional and angle-ply glass fibre / carbon fibre hybrid laminates Riso-R-1168* (Materials research department, Riso DK)
- [11] Zhang Z and Hartwig G 2002 Relation of damping and fatigue damage of unidirectional fibre composites *Int. J. Fatigue* **24** 713–8
- [12] Yin-tao W, Liang-jin G and Ting-qing Y 2001 Prediction of the 3-D effective damping matrix and energy dissipation of viscoelastic fiber composites *Compos. Struct.* **54** 49–55
- [13] Kenny J M and Marchetti M 1995 Elasto plastic behavior of thermoplastic composite laminates under cyclic loading *Compos. Struct.* **32** 375–82
- [14] Audenino A, Crupi V and Zanetti E 2003 Correlation between thermography and internal damping in metals *Int. J. Fatigue* **25** 343–51
- [15] Saravanos D A and Hopkins D A 1996 Effects of delaminations on the damped dynamic characteristics of composite laminates: analysis and experiments *J. Sound Vib.* **192** 977–93
- [16] White D 2004 *New Method for Dual-Axis Fatigue Testing of Large Wind Turbine Blades Using Resonance Excitation and Spectral Loading* (NREL/TP-500-35268)
- [17] Adams R 1986 A review of the damping mechanisms in advanced fibre-reinforced composites *Damping 1986 Proceedings* (Air Force Wright Aeronautical laboratories) p FG–1
- [18] Lemaître J and Desmorat R 2005 *Engineering Damage Mechanics* (Berlin/Heidelberg: Springer-Verlag)
- [19] Wong A K and Kirby G C 1990 A hybrid numerical/experimental technique for determining the heat dissipated during low cycle fatigue *Eng. Fract. Mech.* **37** 493–504
- [20] Bergman T L, Incropera F P, Lavine A S and DeWitt D P 2007 *Fundamentals of Heat and Mass Transfer* (John Wiley & Sons, Ltd)
- [21] Echtermeyer A, Engh B and Buene L 1995 Lifetime and young's modulus changes of glass/phenolic and glass/polyester composites under fatigue *Composites* **26** 10–6

- [22] Cugnet D, Hauviller C, Kuijper A, Parma V and Vandoni G 2002 Thermal conductivity of structural glass/fibre epoxy composite as a function of fibre orientation *19th International cryogenic engineering conference ICEC19* (Grenoble, France)
- [23] Khandelwal M and Mench M M 2006 Direct measurement of through-plane thermal conductivity and contact resistance in fuel cell materials *J. Power Sources* **161** 1106–15
- [24] Anon 2012 EcoTherm insulation datasheet
- [25] Cormier L, Nijssen R and Raijmaekers S 2012 Temperature and frequency effects on the fatigue properties of unidirectional glass fiber-epoxy composites *53RD AIAA* (Honolulu, Hawaii)